MBoC | ARTICLE

Recovery of plasma membrane tension after a hyperosmotic shock

Jasmine Phan[a], Malan Silva[a,b,†], Robin Kohlmeyer[a,c], Romy Ruethemann[a], Lincoln Gay[a], Erik Jorgensen[a,b], and Markus Babst[a,*]

[a]Henry Eyring Center for Cell and Genome Science, University of Utah, Salt Lake City, 84112 UT; [b]School of Biological Sciences, Howard Hughes Medical Institute, University of Utah, Salt Lake City, 84112 UT; [c]University of Osnabrueck, Osnabrueck 49074, Germany

ABSTRACT **Maintaining proper tension is critical for the organization and function of the plasma membrane. To study the mechanisms by which yeast restores normal plasma membrane tension, we used a microfluidics device to expose yeast to hyperosmotic conditions, which reduced cell volume and caused a ∼20% drop in cell surface area. The resulting low tension plasma membrane exhibited large clusters of negatively-charged glycerophospholipids together with nutrient transporters, suggesting phase segregation of the membrane. We found that endocytosis was blocked by the phase segregation and thus was not involved in removing excess membrane. In contrast, rapid recovery of plasma membrane tension was dependent on 1) eisosome morphology changes that were able to absorb most of the excess surface area and 2) lipid transport from the plasma membrane to the endoplasmic reticulum (ER), where lipids were shunted into newly formed lipid droplets.**

SIGNIFICANCE STATEMENT

- Cells often have to rapidly change the surface area. How the plasma membrane maintains proper function under these changing conditions is poorly understood.
- Using hyperosmotic treatment, the authors showed that cells respond to shrinking and the resulting low plasma membrane tension by change in surface morphology and by lipid transport from the plasma membrane to the ER.
- The study identifies mechanisms that are involved in maintaining proper membrane tension, a parameter that affects all aspects of plasma membrane–associated functions.

Monitoring Editor
Matthew Welch
University of California, Berkeley

Received: Oct 1, 2024
Revised: Feb 10, 2025
Accepted: Feb 12, 2025

This article was published online ahead of print in MBoC in Press (http://www.molbiolcell.org/cgi/doi/10.1091/mbc.E24-10-0436) on February 19, 2025.

†Present address: Janelia Research Campus, Howard Hughes Medical Institute, Ashburn, 20147 VA.

Author contributions: J.P., E.J., and M.B. conceived and designed the experiments; J.P., M.S., R.K., R.R., L.G., and M.B. performed the experiments; J.P., M.S., R.K., R.R., L.G., and M.B. analyzed the data; J.P. and M.B. drafted the article; M.B. prepared the digital images.

Conflicts of interest: The authors declare no competing financial interests.

*Address correspondence to: Markus Babst (babst@biology.utah.edu).

Abbreviations used: cER, cortical ER; EM, electron microscopy; EPCS, ER-PM contact site; LEDS, large eisosome derived structure; PIP2, phosphatidylinositol 4,5-bisphosphate; PM, plasma membrane; PS, phosphatidylserine.

INTRODUCTION

The plasma membrane (PM) contains numerous proteins that function in nutrient uptake, environmental sensing, and cell signaling. PM physical properties, such as thickness and fluidity, can dramatically affect the organization and activity of these PM-associated proteins. Therefore, it is important that the cell maintains PM properties within a physiological range, even when exposed to rapidly changing environments. One key parameter the cell uses to control fluidity and thickness is membrane tension (Le Roux *et al.*, 2019; Sitarska and Diz-Munoz, 2020). The PM experiences a constant tension that is generated by turgor pressure. The inflow of water molecules (osmosis), exerts an outward force on the PM, which in turn causes membrane tension (Roffay *et al.*, 2021). This tension increases lipid fluidity and lowers organization of lipids and proteins in the PM. Low PM tension is detrimental to the cell and has been shown to affect cell signaling, nutrient transport, and lipid organization of the PM (Riggi *et al.*, 2018; Appadurai *et al.*, 2020; De Belly *et al.*, 2021).

Saccharomyces cerevisiae is particularly well suited for studying PM tension homeostasis, as yeast in the wild accommodates harsh environments with temperature drops and exposure to high concentrations of osmolytes. For example, exposure to salts or high-solute environments draws water out of cells via aquaporins. The result is a decrease in cell volume and PM tension caused by the increased surface area/volume ratio. In response to this hyperosmotic stress, MAPK signaling pathways up-regulate the synthesis of the osmolyte glycerol to reestablish osmotic balance. Glycerol draws water back into the cell to restore normal cell size and thus recover PM tension (Saito and Posas, 2012). Another mechanism that supports the recovery from loss of membrane tension relies on TORC2 inhibition. Low membrane tension causes phase segregation of the PM, which results in the clustering of the lipid phosphatidylinositol 4,5-bisphosphate (PIP2). The PIP2 clusters sequester and inhibit TORC2 activity. As a consequence of TORC2 inhibition, sphingolipid synthesis at the endoplasmic reticulum (ER) is impaired, preventing the delivery of long-chain lipids that might further decrease fluidity (Riggi *et al.*, 2018).

The MAPK- and the TORC2-mediated stress responses require changes in metabolic pathways, both of which are slow responses. In contrast, yeast eisosomes are able to immediately respond to changes in PM tension. Eisosomes are membrane furrows ~50 nm deep and ~300 nm long. These membrane folds are formed in part by a polymer of the BAR domain proteins Pil1 and Lsp1 (Douglas and Konopka, 2014). Changes in PM tension have been shown to affect the size of the eisosomes. High tension causes the flattening of the eisosomes whereas low tension increases both depth and length of these membrane structures (Kabeche *et al.*, 2015; Appadurai *et al.*, 2020; Ng *et al.*, 2020; Lemiere *et al.*, 2021). Therefore, eisosomes seem to provide or absorb cell surface area in order to maintain proper PM tension.

Our study focused on the acute phase (seconds to minutes) of hyperosmotic shock and its effect on the organization and function of the PM. We found that the acute loss of PM tension resulted in an endocytosis block and in the clustering of lipids and proteins in large eisosome-derived structures (LEDS). Recovery from this membrane stress involved PM morphology changes and lipid transfer from the PM to the cortical ER.

RESULTS

To better understand how yeast responds to loss of PM tension, we analyzed the morphology and organization of the PM after the addition of 1M sorbitol to the growth medium. Sorbitol is a sugar that raises the osmolarity of the medium without affecting ion gradients or the cell's metabolism. To observe the immediate consequences of hyperosmotic shock, we visualized yeast by fluorescence microscopy in a microfluidics chamber that maintains optimal growth conditions and allows for quick changes in the environment. Most importantly, using the microfluidics system, we observed the same cells before and after treatment, eliminating some of the problems caused by cell-to-cell variability. To visualize the PM, cells expressed a mutant form of the GFP-tagged nutrient transporter Fur4 that lacks the N-terminal ubiquitination sites and, therefore, remains stable at the PM (Fur4ΔN-GFP; Keener and Babst, 2013). Using the GFP signal as the boundary of the cell, we measured the diameter of the cell to determine cell size changes at different timepoints. These data indicated that cells shrink rapidly during hyperosmotic shock (0M>1M sorbitol), reducing their surface area within the first 2 min by 22% (median; surface calculation assumes a spherical cell; Figure 1, A and B). This observation was consistent with previous observations that hyperosmotic shock induced excretion of water via aquaporins (Pettersson *et al.*, 2005). After 20 min, the cell surface area recovered to ~40% of the initial size, likely due to cell adaptation by the synthesis of osmolytes such as glycerol (Blomberg, 2022). Consistent with this idea, we observed that cells that were depleted for nutrients 3 min before the hyperosmotic shock and therefore were not able to synthesis osmolytes, did not recover in size (SD minus glucose and amino acids; Figure 1A).

Low PM tension impairs endocytosis

We predicted that the rapid cell shrinking we observed during acute hyperosmotic shock would cause an excess of membrane that would create low tension or membrane slack on the PM. Endocytosis would be an obvious mechanism for removing the excess membrane from the cell surface. Furthermore, we expected that low membrane tension would allow for easier deformation of the PM and, thus, for faster formation of endocytic structures. To our surprise, we found that hyperosmotic shock blocked endocytosis. For these experiments, we quantified the internalization rate of the methionine transporter, Mup1, both under normal growth conditions and during acute hyperosmotic shock. To trigger Mup1 endocytosis, we switched the cells in the microfluidics system from a growth medium without methionine to a medium that contained 0.5 mg/ml methionine (Figure 1C). Quantification of substrate-induced downregulation of Mup1 indicated that the addition of 1M sorbitol delayed the endocytic response by 10 to 12 min (Figure 1D). This observation suggested that low PM tension blocks endocytosis and that endocytosis does not play a role in the removal of excess membrane during the initial phase of hyperosmotic stress. Furthermore, this result highlighted the importance of maintaining proper membrane tension to allow for normal PM-associated functions.

Hyperosmotic shock changes eisosome morphology

The yeast PM contains invaginated membrane furrows, referred to as eisosomes, that share similarities with the mammalian caveolae. Eisosomes represent specialized membrane domains that store APC-type nutrient transporters such as Fur4 (Moharir *et al.*, 2018). Furthermore, eisosomes have been implicated in regulating the tension of the PM by changing their size and thus providing or storing membrane (Appadurai *et al.*, 2020). Because hyperosmotic shock reduces PM tension, we analyzed potential changes in eisosome morphology by visualizing the eisosome protein

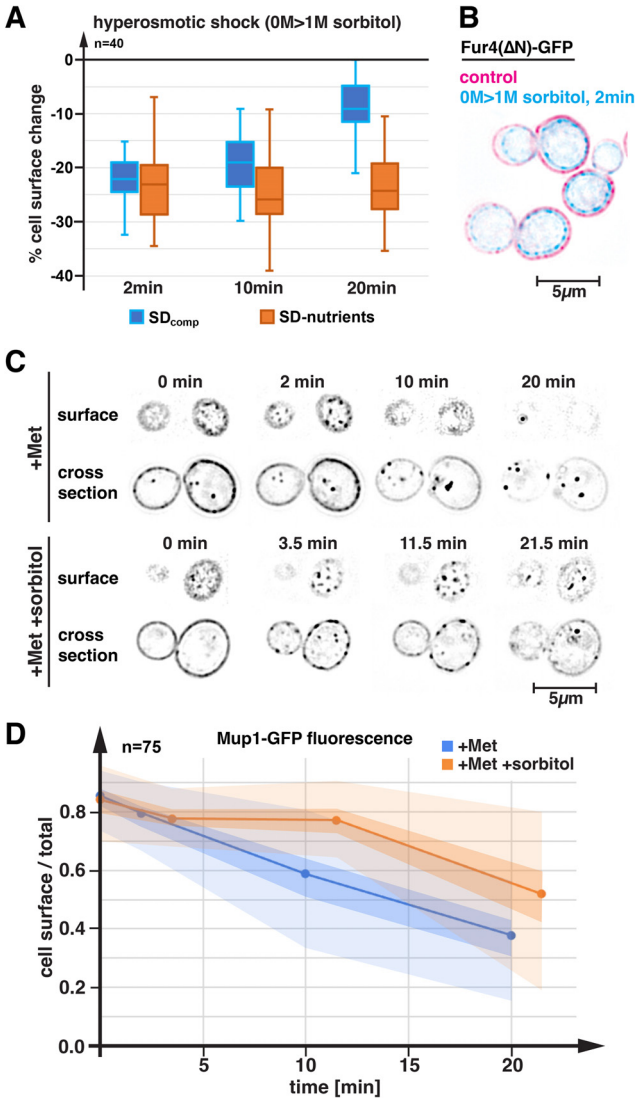

FIGURE 1: Hyperosmotic shock causes cell shrinking and a block in endocytosis. (A) WT cells expressing Fur4(ΔN)-GFP (SEY6210 pJK30) were observed in a microfluidics chamber during the hyperosmotic shock (addition of 1M sorbitol to the medium) and the changes in cell surface area was determined by measuring the diameter of mother cells at different timepoints (assuming a spherical shape of the cells). These experiments were done either in presence of SD_{comp} medium or 3 min after shifting cells to medium lacking any carbon source (SD-nutrients). The data are presented as a box-and-whisker plot, marking the mean. (B) Example of cells before (control) and after hyperosmotic shock (0M>1M sorbitol). (C) WT expressing Mup1-GFP (BWY3817) grown in absence of methionine was observed in a microfluidics chamber after addition of methionine (20 mg/l), either in presence or absence of 1M sorbitol. (D) Quantification of the experiment shown in C. The dots mark the median and the shaded areas indicate the quartiles and extremes of the data set (box and whisker plot, $n = 75$).

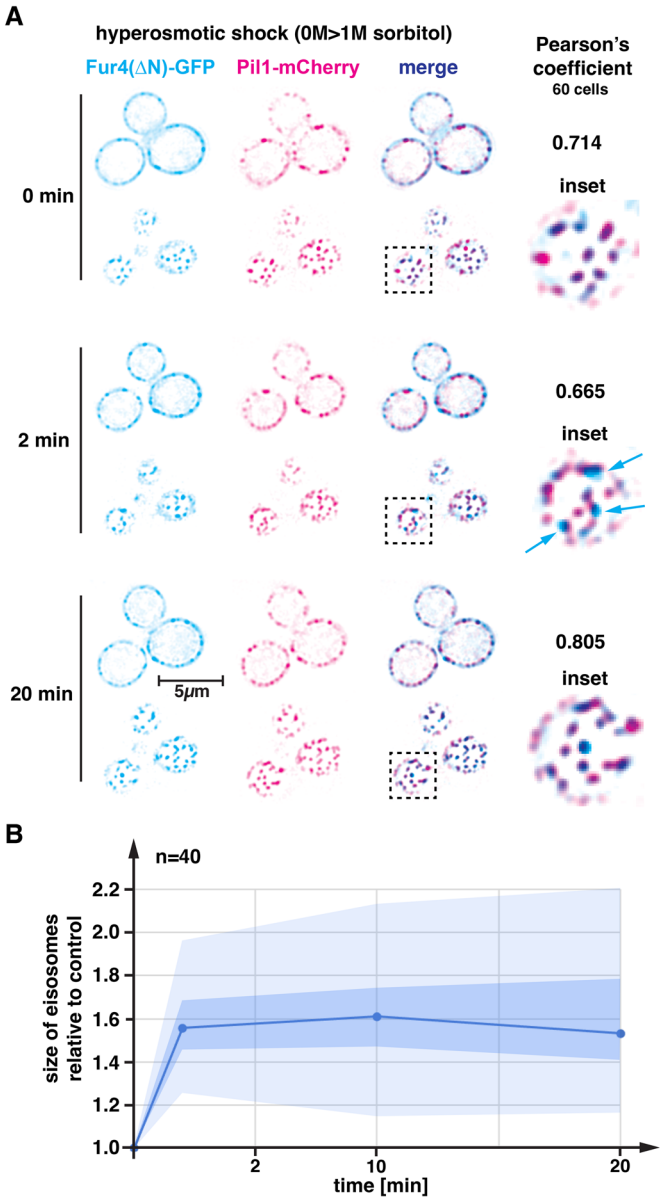

FIGURE 2: Hyperosmotic shock changes the morphology and size of eisosomes. (A) Microfluidics-based analysis of hyperosmotically treated WT cells expressing Fur4(ΔN)-GFP and Pil1-mCherry (AMY6 pJK30). Each timepoint shows a cross-section and a surface view of the cells. Arrows indicate enlarged Fur4(ΔN)-GFP containing membrane domains that only partially colocalize with the eisosomal marker Pil1-mCherry. (B) Quantification of the pixels occupied by Pil1-mCherrry before and after hyperosmotic shock. Because the number of eisosomes does not change, an increase in pixels indicated and increase in size of eisosomes. The dots mark the median and the shaded areas indicate the quartiles and extremes of the dataset (box and whisker plot, $n = 40$).

Pil1-mCherry and the eisosome-associated protein Fur4ΔN-GFP. As expected, the microscopy analysis showed that concomitant with the initial rapid cell shrinking, eisosomes changed morphology and increased in length (Figure 2A; see also Figure 3B). As a consequence, the surface area occupied by Pil1-mCherry increased 1.6-fold in <10 min (number of Pil1-mCherry pixels; Figure 2B).

The membrane domain occupied by Fur4 also increased in size, and many of these structures expanded beyond the Pil1-marked eisosomes (see arrows in Figure 2A). As a result, the Pearson's coefficient for Pil1-Fur4 colocalization was reduced 2 min after hyperosmotic shock (Figure 2A). Twenty minutes after hyperosmotic shock, the cells not only recovered most of their size (Figure 1A), but also Fur4 had restored localization to eisosomes (Figure 2A). Eisosomes, however, did not return to their original size and

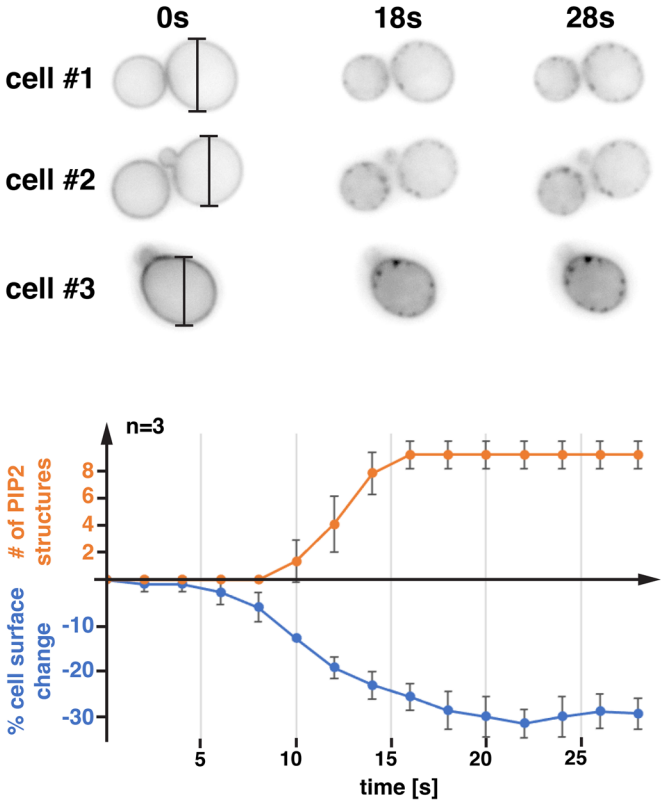

FIGURE 3: Hyperosmotic shock causes rapid clustering of PIP2. Time-lapse imaging (picture every 2 s) of WT cells expressing a GFP-tagged PIP2-binding protein (SEY6210 pCS189) during hyperosmotic shock. Three cells were chosen for quantification of surface area (based on diameter indicated in 0 s picture) and number of PIP2 dots.

remained enlarged (Figure 2B). Together, our observations were consistent with the proposed role of eisosomes in membrane tension control. The increase in eisosome size allowed these furrows to store more membrane and thus counter some of the membrane tension loss.

Low PM tension causes the formation of LEDS

A previous publication observed that low PM tension caused the clustering of lipid phosphatidyl-4,5-bisphosphate (PIP2), possibly by lipid phase segregation (Riggi *et al.*, 2018). We repeated these experiments in the microfluidics system, using cells expressing a GFP-tagged PIP2 sensor, and we observed the same clustering of PIP2 after shifting the cells to hyperosmotic conditions (Figure 3). PIP2 clustering started ~4 s after the first indication of cell shrinking (at ~10% cell surface reduction) and was completed 8 s later. This very rapid response to the loss of membrane tension was consistent with the idea that the formation of PIP2 clusters was caused by phase segregation. Following cells for 20 min after hyperosmotic shock (Figure 4A), we observed the diffusion of the initially formed PIP2 clusters. Quantification of the microscopy data showed that the disappearance of the PIP2 clusters was faster than the cell size recovery (Figure 4C). At 10 min of hyperosmotic conditions, the cell surface area recovered only by 25%, whereas 65% of the PIP2 clusters had dissolved at this timepoint. Similarly, at the 20 min timepoint, PIP2 clusters were almost all dissolved, whereas cell size recovered by 50%. This observation suggested that membrane tension recovery was not only mediated by glycerol-induced cell swelling but also involved additional mechanisms.

To understand the localization of these lipid clusters, we colocalized PIP2 clusters with the eisosome marker Pil1-mCherry. The observed PIP2 clusters partially colocalized Pil1-mCherry, and similar to Fur4ΔN-GFP, extended beyond the eisosomes (see arrows in Figure 4B). Colocalization studies using cells expressing the mCherry-tagged PIP2 sensor and Fur4ΔN-GFP confirmed that after hyperosmotic shock, the two clusters overlapped but were not identical in size and morphology (Figure 5A). The larger Fur4-GFP clusters often bordered the PIP2 structures (see enlarged inset in Figure 5A). We also tested the effect of hyperosmotic conditions on the methionine transporter Mup1 that, similar to Fur4, transiently associates with eisosomes (Moharir *et al.*, 2018). After the hyperosmotic shock, Mup1-GFP showed almost perfect colocalization with the PIP2 structures (Figure 5B). However, it should be noted that a pool of Mup1-GFP remained diffusely distributed across the cell surface. Similarly, the lipid phosphatidylserine (PS), which is enriched in the cytoplasmic leaflet of the PM, partially clustered during hyperosmotic shock into structures that colocalized with the PIP2 structures (Figure 5C).

In summary, the two negatively charged phospholipids of the plasma membrane, PS and PIP2, assemble during acute hyperosmotic shock with APC-type nutrient transporters into large membrane domains that partially overlap with the eisosomal marker Pil1. We propose that these lipid-protein clusters represent enlarged eisosomal membrane domains, which we call LEDS. During normal membrane tension, eisosome components dynamically exchange with the surrounding, more fluid membrane environment and transiently localizing to eisosomes. However, loss of membrane tension causes phase segregation of the PM and, as a result, the accumulation and expansion of the eisosomal membrane. It is likely that even under normal growth conditions, PS and PIP2 are concentrated in eisosomes. However, this lipid enrichment is not detectable because the eisosome-associated Pil1/Lsp1 polymer that is known to bind to negative charged lipids blocks access of the PS and PIP2 sensors to the lipids. This idea is consistent with recent electron microscopy (EM)-based studies of eisosomes that indicated an enrichment of PIP2 and PS in these membrane domains (Kefauver *et al.*, 2024; Tsuji *et al.*, 2025).

The morphology of PM at low tension

We further analyzed the PM morphology of hyperosmotic-shocked cells by transmission EM. In untreated wild-type (WT) cells, we quantified an average of ~29 eisosome-like structures per cell, which were defined as ~50 nm deep furrows in the PM (Figures 6, A, F, and G). This number was generated based on the observed number of structures per μm^2, the average surface area of yeast cells (68 μm^2, based on light microscopy) and the estimated length of eisosomes ~300 nm (Stradalova *et al.*, 2009). Most of these structures are likely eisosomes, but we cannot exclude the possibility that some of these eisosome-like structures are endocytic pits. The estimated number of eisosomes doubled in the first 5 min after hyperosmotic treatment (Figure 6G), which was consistent with the fluorescence microscopy data that indicated an increase in the surface area occupied by Pil1 (Figure 2B). After 10 min of hyperosmotic shock, we found another 1.6-fold increase in the number of eisosome-like structures by EM that was not observed by fluorescence microscopy (compare Figures 6G and 2B). We suspected that this increase in eisosome-like invaginations might in fact represent the formation endocytic pits that form when endocytosis is reactivated ~10 min after treatment with sorbitol (see Figure 1D).

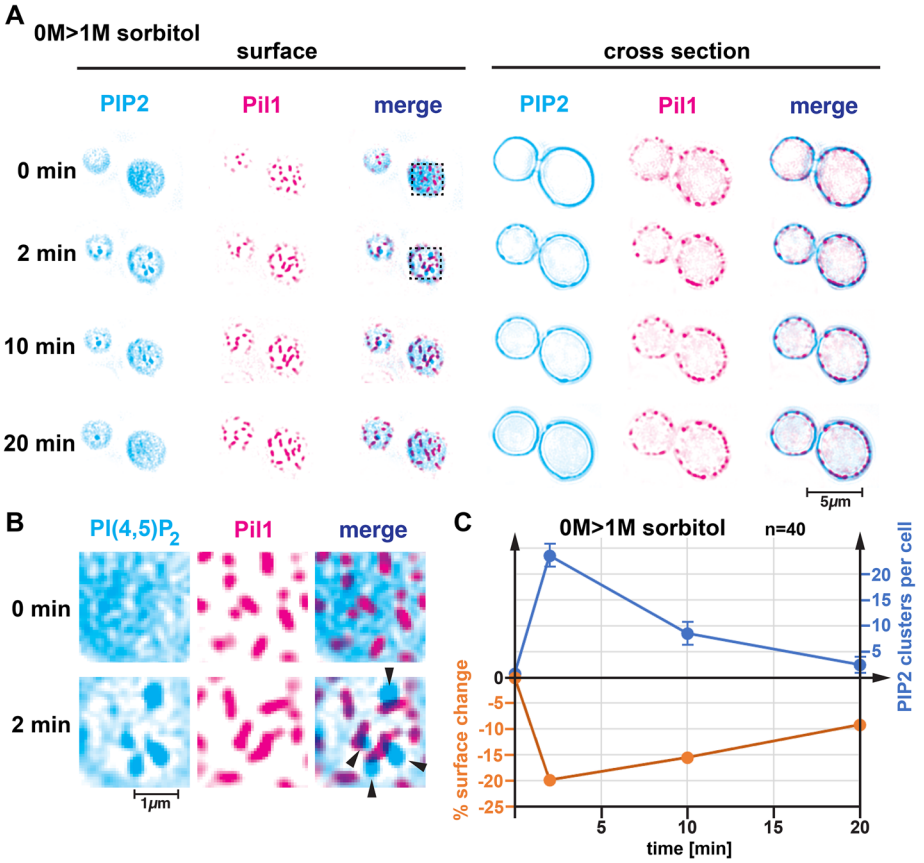

FIGURE 4: Loss of membrane tension results in PIP2 clustering. (A) WT yeast expressing GFP-tagged PIP2 sensor and Pil1-mCherry (AMY6 pCS189) was exposed in a microfluidics chamber to hyperosmotic conditions (addition of 1M sorbitol to the medium). (B) Enlarged surface areas of a cell before and 2 min after hyperosmotic shock (see marked areas in A). Arrows indicate large PIP2 clusters that partially overlap with eisosomes. (C) Quantification of the number of PIP2 clusters (median, SD) and surface area change (mean).

Unlike the control samples (Figure 6A), cells treated with 1M sorbitol for 1 min exhibited large structures that appeared to be extracellular vesicles (arrows in Figure 6B). Based on the similarity in staining, the vesicle-like structures appeared to contain cytoplasm. We also observed cortical ER in ~60% of the structures (cER; Figures 6D), suggesting that these structures were likely still connected to the cell and not detached extracellular vesicles. Quantitative analysis of the EM micrographs indicated the formation of ~29 vesicle-like structures per cell (1 min timepoint in Figure 6G), which corresponded with the ~24 PIP2 clusters observed by fluorescence microscopy (see Figure 4C). Both the vesicle-like structures and the PIP2-marked LEDS were short-lived, with at least half of both LEDS and vesicle structures being resolved during the first 10 min of hyperosmotic shock (Figures 4C and 6G). These similarities hinted that vesicle-like structures and LEDS might represent the same PM structure.

To test this idea, we stained cells with the membrane dye FM4-64, which fluoresces when intercalated into the outer leaflet of the PM. Because the vesicle-like structures add two additional layers of membranes to the cell surface (see morphology in Figure 6D), we expected that FM4-64 would label these structures up to 3x brighter when compared with the rest of the PM. Indeed, hyperosmotic-treated cells showed the rapid formation of FM4-64 structures at the cell surface that were in average 2.2x brighter than the surrounding membrane (Figures 7, A–C). These FM4-64 spots partially overlapped with Pil1 (Figures 7, A and B) and colocalized with PIP2 (Figure 7D), suggesting that they labeled LEDS. Cells deleted for *pil1Δ and* stained with FM4-64 showed aberrant plasma membrane structures before the hyperosmotic shock (Figure 7E), which is consistent with the previously reported eisosome remnants in this mutant strain (Walther *et al.*, 2006). After the hyperosmotic shock, the eisosome remnants of *pil1Δ* were enlarged. Some additional structures were observed, but most did not match the morphology of LEDS (arrows in Figure 7E). Notably, there was a lack of even distribution of FM4-64 clusters, further supporting the model that LEDS are eisosome-derived structures. Together, the FM4-64 data were consistent with the by EM observed morphology and thus suggested that the vesicle-like structures observed by EM corresponded to the LEDS identified by fluorescence microscopy.

Figure 8A explains our model for the formation of LEDS. We propose that loss of membrane tension causes the rapid expansion of the raft-like eisosome membrane domain, thereby increasing the clustering of negatively charged lipids and APC transporters. As a result, the eisosome expands inward and bends back toward the PM, either because of contacts between eisosomes and the cER (Ng *et al.*, 2020) or because the eisosome membrane domain expands asymmetrically, accumulating new lipids mainly on one side of the furrow. The expanding furrow then contacts and fuses with the PM, forming a membrane tube. This PM tube is surrounded by extracellular space where the open space of the furrow expanded. The resulting morphology can be best described as a "recessed

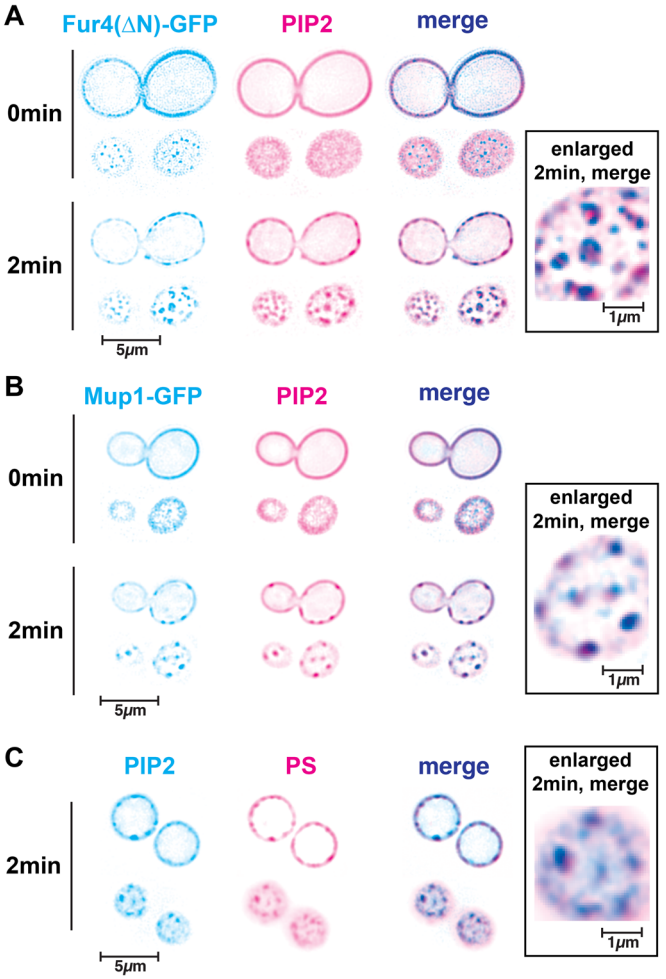

FIGURE 5: Hyperosmotic-induced clustering of nutrient transporters with negatively charged lipids. The experiments were performed in a microfluidics chamber and pictures were taken before and 2 min after addition of 1M sorbitol to the growth medium. (A) WT cells expressing Fur4(ΔN)-GFP and RFP-tagged PIP2 sensor (SEY6210 pJK30 p1776). (B) WT cells expressing Mup1-GFP and RFP-tagged PIP2 sensor (SEY6210 pPL4146 p1776). (C) WT cells expressing GFP-tagged PIP2 sensor and RFP-tagged PS sensor (SEY6210 pCS189 pLACT2C2).

handle" (Figure 8C). As a result of the membrane fusion, the Pil1 polymer that originally localized to the tight bend of the eisosome is now positioned at the edge of the LEDS and forms a new and extended eisosome (Figures 8, A and B). This model is supported by the presence of other PM structures observed by EM of hyperosmotically treated cells. For example, Figure 6C shows deep invaginations of the PM that might represent an intermediate morphology in the LEDS formation process. The PM structure in Figure 6E might show a longitudinal section through the proposed membrane tube of LEDS. This type of structure was only found twice among ~40 cross-sections of hyperosmotically treated yeast but was not observed in the controls (untreated). The rarity of these structures can be explained by the elongated morphology of the membrane tubes, which, in most cutting angles, will result in circular/oval cross-sections in EM imaging. Together, our model of LEDS formation is consistent with the observations we obtained both by fluorescence and EM.

In summary, we propose that the loss of PM tension caused a rapid expansion of the eisosomal furrows, both in length and depth. The fusion of these extended and bent eisosomes with the PM results in the formation of membrane tubes or LEDS. These morphology changes of the PM allow the cell to temporarily reorganize excess membrane. Based on our EM observations, we estimated that LEDS, together with the enlarged eisosomes, store ~15% additional surface area (assuming the transformation of 30 eisosomes into 30 LEDS). Additional surface area might be stored in the deep invaginations we observed in the hyperosmotically treated cells (Figure 6, C and F), the identity of which is discussed below.

Endocytosis mutants exhibit PM tension problems

The EM analysis of WT cells identified deep invaginations of the plasma membrane that formed within the first minute of hyperosmotic shock (Figure 6C). Some of these structures might be extended eisosomes that did not fuse to the plasma membrane and thus did not form LEDS, whereas other structures might represent endocytic sites that increased in size because of the slack membrane and/or the block in endocytosis. Consistent with the latter idea, endocytosis mutants have been previously shown to form cargo-containing, deep endocytic structures (Wendland *et al.*, 1996). To test whether these deep invaginations could represent stalled endocytic structures, we visualized an *end3*Δ mutant strain, which lacks a nonessential subunit of the endocytic coat that helps initiate the actin cytoskeleton at endocytic pits (Benedetti *et al.*, 1994). EM analysis of this strain showed a large number of the deep invaginations even before hyperosmotic shock, supporting the idea that most of these structures are indeed aberrant endocytic pits (Figure 9A). Furthermore, the EM analysis of the *end3*Δ mutant identified an increased number of eisosome-like structures (~1.4-fold over WT; Figure 9B). Together, these observations suggested that the *end3*Δ cells have reduced PM tension even under normal growth conditions.

Sorbitol treatment of *end3*Δ cells showed the rapid formation of LEDS, that by EM were more commonly observed in the mutant cells than in WT (~1.6 over WT; Figure 9C). However, 10 min after the hyperosmotic shock, the number of both LEDS and deep invaginations were similar to that of WT (Figure 9, C and D), suggesting that in *end3*Δ the stress response system restored PM tension to normal levels, beyond the starting conditions.

It is interesting to note the accumulation of secretory vesicles in the micrographs of *end3*Δ mutant cells (Figure 9A), consistent with the idea that membrane tension also plays an important role in the membrane fusion process (Kozlov and Chernomordik, 2015). Therefore, *end3*Δ cells not only exhibit a defect in endocytosis, but also in secretion (Rollenhagen *et al.*, 2022). This PM tension–based link between endocytosis and secretion might be the mechanism by which the cell maintains homeostatic balance of these two opposing pathways.

Hyperosmotic shock causes the formation of lipid droplets

When we compared the EM micrographs of WT cells before and after the addition of sorbitol (Figure 6, A and B), we noticed an increase in the numbers of lipid droplets (LDs) in hyperosmotic-treated cells. We confirmed this finding by fluorescence microscopy of BODIPY-stained cells. For these experiments, we grew cells in medium with galactose as the carbon source, which in comparison to glucose-grown cells reduced the size and number of LDs (all experiments in Figure 10 were using galactose-grown yeast). These cells were either shifted to normal growth medium (control)

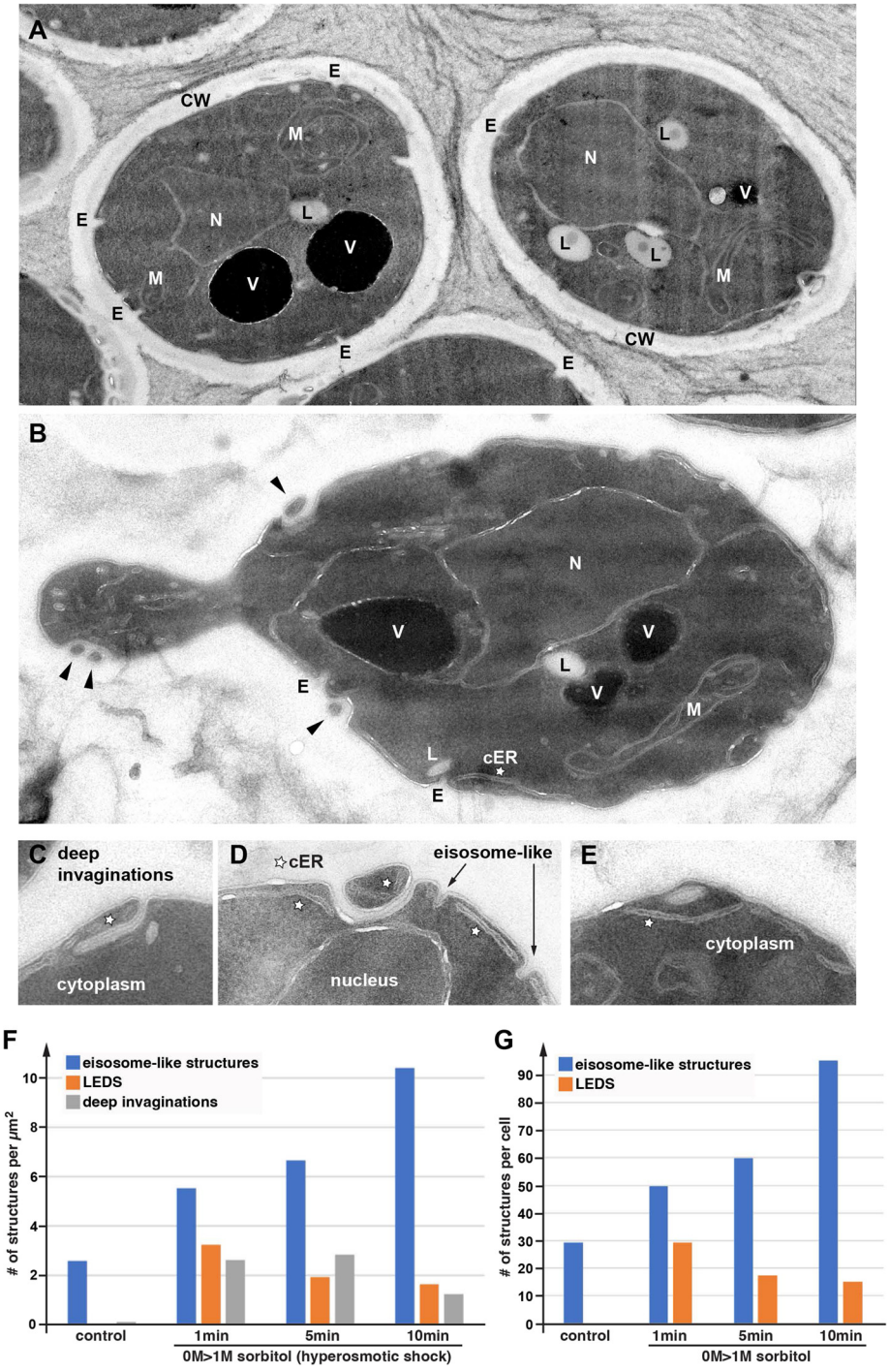

FIGURE 6: Changes in PM morphology caused by low membrane tension. WT cells were visualized by transmission EM before (A) or after addition of 1M sorbitol (B–E, 1 min treatment). Labels: N, nucleus; V, vacuole; L, lipid droplet; M, mitochondria; E, eisosome; CW, cell wall; star marks cER; arrow heads mark LEDS. (F, G) Quantification of the by EM observed structures (based on 40 cell sections of 50 nm thickness).

or to hyperosmotic conditions (growth medium +1M sorbitol) and the number of LDs was quantified after 20 min using BODIPY staining. We counted the formation of ~6 additional LDs per cell (from ~9 to ~15; WT in Figure 10A). Using Erg6-GFP as a marker for LDs (Leber *et al.*, 1994), we observed that hyperosmotic-induced LD formation was rapid and that most of these newly formed LDs were temporary. Maximal LD formation was reached at 5 min and the number of ERG6-GFP puncta started to drop 20 min after the stress (Figure 10B). Furthermore, the microscopy showed that the newly formed LDs often localized to the periphery of the cell and were smaller than most of the LDs in untreated cells (Figure 10C).

Given that we observed cER present at many LEDS (Figure 6D) we tested whether formation of new LDs during hyperosmotic shock was dependent on eisosomes or LEDS. Surprisingly it was

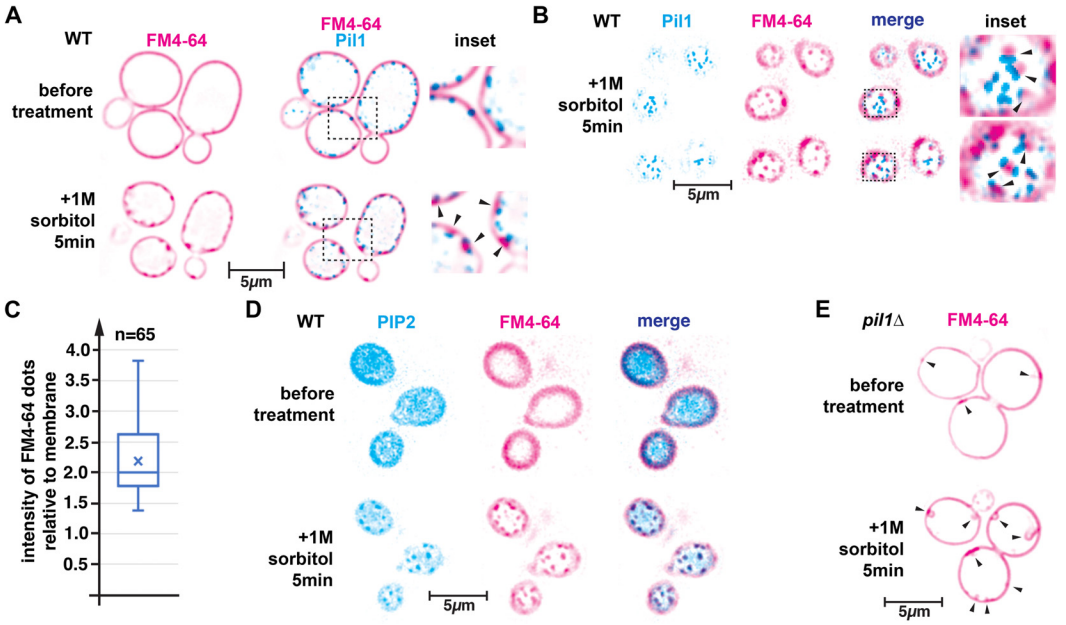

FIGURE 7: FM4-64 marks the LEDS of hyperosmotically treated cells. (A, B) FM4-64 staining of WT expressing Pil1-GFP (AMY10) in a microfluidics chamber, before and 5 min after addition of 1M sorbitol. (A) shows cross-sections, whereas (B) shows the surface of the cells. (C) Quantification of the FM4-64 signal of LEDS compared with the signal of the surrounding membrane. (D) FM4-64 staining in the microfluidics chamber of WT cells expressing a GFP-tagged PIP2 sensor. The pictures show the surface of the cells before and after sorbitol treatment. (E) FM4-64–stained *pil1*Δ mutant cells (AMY42) were visualized in a microfluidics chamber, before and after hyperosmotic stress.

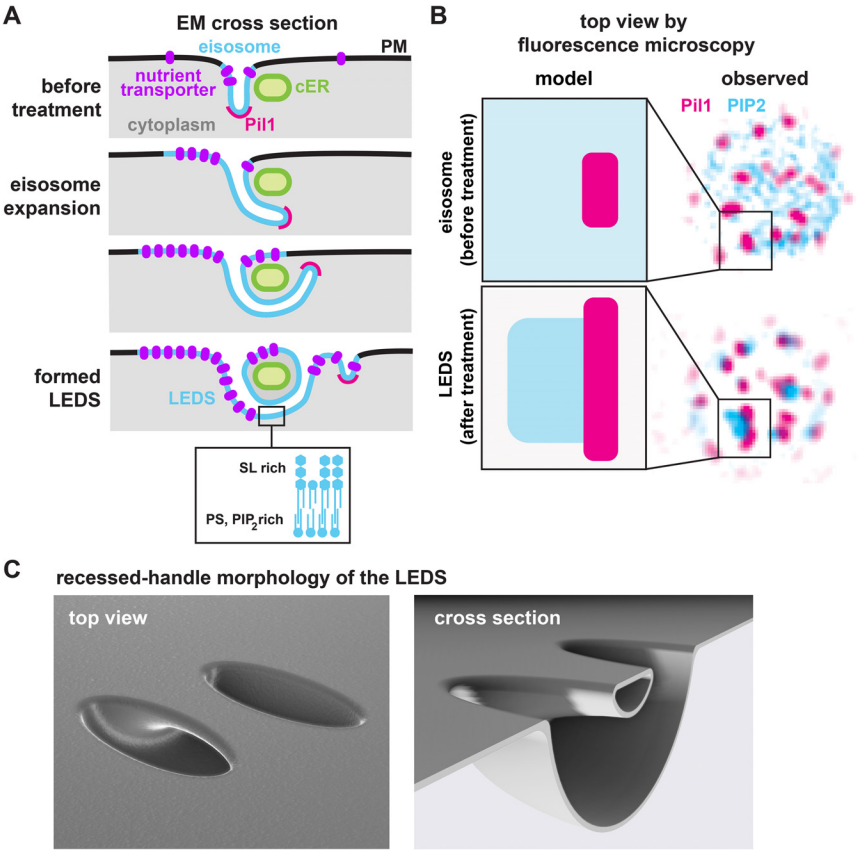

FIGURE 8: Model of the formation and morphology of LEDS. (A) Model of the transformation of eisosomes to LEDS (SL, sphingolipids). (B) Explanation of the by fluorescence microscopy observed changes in eisosome morphology and PIP2 localization. (C) Three-dimensional model of the proposed morphology of LEDS.

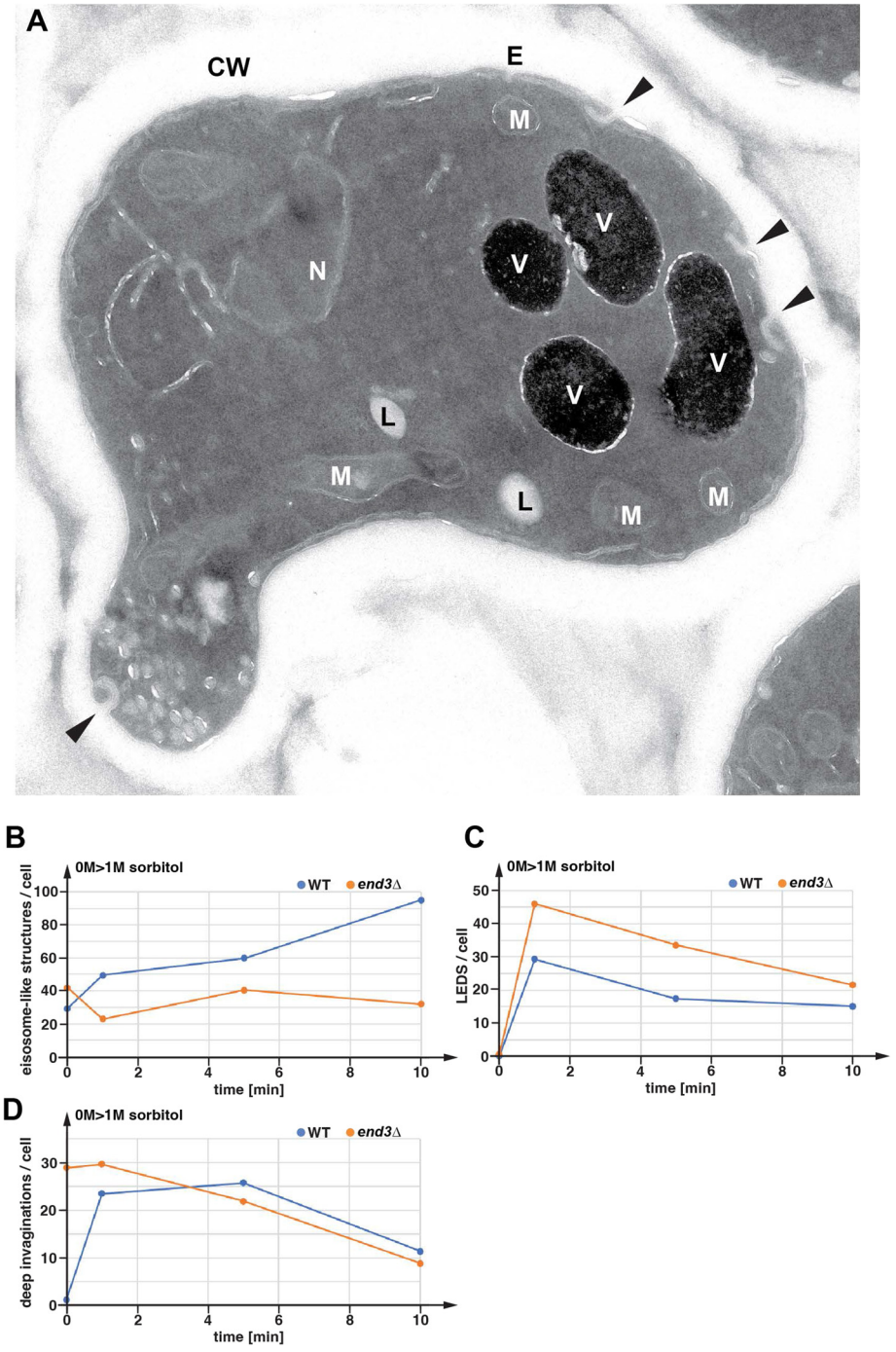

FIGURE 9: Endocytosis mutants exhibit phenotypes of low PM tension. Cells mutated for *END3* (BWY1346) were analyzed by EM (50 nm sections). (A) Example of an *end3*Δ cell before sorbitol treatment (control). Arrows indicate deep invaginations (labels: CW, cell wall; V, vacuole; N, nucleus; M, mitochondria; L, lipid droplet). (B–D) Quantification of the observed structures based on 40 cell sections. The WT data are identical to the data shown in Figure 6.

not (see *pil1*Δ in Figure 10A), but it did require the membrane contact site proteins Scs2/Scs22 (Figure 10A). At the ER-PM contact sites, Scs2/22 function in the recruitment of Osh2 and Osh3, two homologues lipid binding proteins that have been implicated in the lipid transfer from the ER to the PM. Consistent with this, deletion of either *OSH2* or *OSH3* resulted in a defect in osmotic stress induced LD formation (Figure 10A), suggesting that during hyperosmotic conditions Osh2/3 might function in the transport of lipids from the PM to the cER where these lipids are subsequently shunted into LDs. This postulated lipid transfer was specific for the Scs2/22-Osh2/3 system and did not include the tricalbins, another family of lipid transfer proteins localized to the ER-PM contact sites (*tcb1/2/3*Δ triple mutant in Figure 10A; Qian *et al.*, 2021).

Scs2/22 together with the Osh2/3 proteins are known to form a complex that is predicted to deliver lipids from the cER to forming endocytic pits under normal growth conditions. This lipid delivery

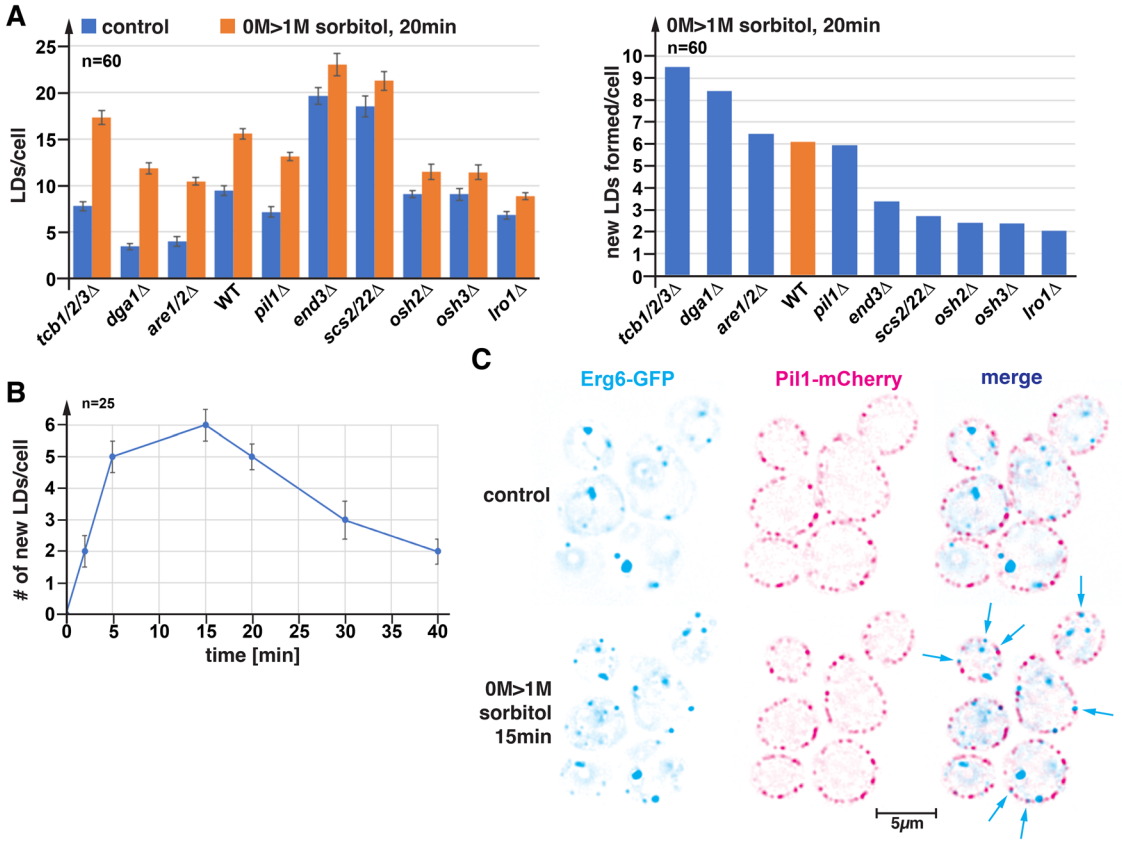

FIGURE 10: Hyperosmotic shock causes the rapid formation of additional LDs. (A) The LDs of different yeast strains before and after hyperosmotic shock were labeled with BODIPY and counted. The bar graph shows the average number and the standard error. The following strains were used: JPY45 (*tcb1/2/3*Δ), JPY22 (*dga1*Δ), JPY47 (*are1/2*Δ), SEY6210 (WT), AMY42 (*pil1*Δ), BWY1346 (*end3*Δ), JPY15 (*scs2/22*Δ), MTY42 (*osh2*Δ), MTY43 (*osh3*Δ), JPY23 (*lro1*Δ). (B) WT expressing Erg6-GFP (JPY35) was treated in a microfluidics chamber with 1M sorbitol and the number of newly formed LDs was monitored over time (graph shows median, ± standard error). (C) Microscopy pictures of WT cells expressing Erg6-GFP and Pil1-mCherry (JPY38) observed in a microfluidics chamber before and after hyperosmotic shock (single optical section). The arrows indicate newly formed LDs.

system aids in the polymerization of actin and the formation of endocytic vesicles (Encinar Del Dedo *et al.*, 2017). The LD formation we observed during acute PM slack seems to be mediated by the same Scs2/22-Osh2/3 system. Consistent with this idea, we observed a ~2-fold reduction in hyperosmotic-induced LD formation in *end3*Δ mutant cells (Figure 10A), which suggested a functional link between the endocytic machinery and the proposed PM-to-cER lipid transport. It is possible that the Osh2/3-mediated removal of lipids at endocytic pits allows for a faster recovery of endocytosis during hyperosmotic stress.

To identify the type of lipids that were stored in the newly formed LDs after hyperosmotic shock, we tested strains deleted for the known lipid acyltransferases. Yeast expresses two acyltransferases, Dga1 and Lro1, that convert diacylglycerol to triacylglycerols, the main storage lipid in LDs. Furthermore, Are1 and Are2 are specific for the acylation of ergosterol, producing ergosterol-esters that are also stored in LDs. The BODIPY staining of hyperosmotically treated mutants indicated that Lro1, one of the acyltransferases that produces triacylglycerols (Oelkers *et al.*, 2000), was necessary for formation of new LDs. In contrast, Dga1, Are1, and Are2 were not involved in the PM stress–induced LD formation (Figure 10A). These results indicated that the newly formed LDs were mainly composed of triacylglycerols, which could suggest that the lipids transported from the PM to the ER during hyperosmotic shock were mostly glycerophospholipids. However, it is also possible that ergosterol is transported to the ER during PM stress and the formation of triacylglycerol-containing LDs are the result of lipid imbalance.

Deletion of PIL1 or OSH2 delays recovery of membrane tension

The data so far suggested that hyperosmotically treated cells recover their membrane tension by changing the morphology of eisosomes and by lipid transport from PM to the cER. We tested whether the loss of these stress response pathways affected the kinetics of restoring normal PM tension. Cell size measurements in the microfluidics system indicated that loss of Pil1 or Osh2 did not change the extent of cell shrinking or the kinetics of cell size recovery (Figure 11A), which suggested that these mutants were not impaired in osmolyte production. In contrast, we observed that the *osh2*Δ mutant strain exhibited a much higher number of PIP2 clusters at 2 min after sorbitol addition and both *osh2*Δ and *pil1*Δ showed a delay in dissolving PIP2 clusters (Figure 11, B and C), indicating that both mutants were impaired in the recovery of normal membrane tension. Together, the mutant analysis supported the idea that the formation of LEDS and lipid transport aid in the

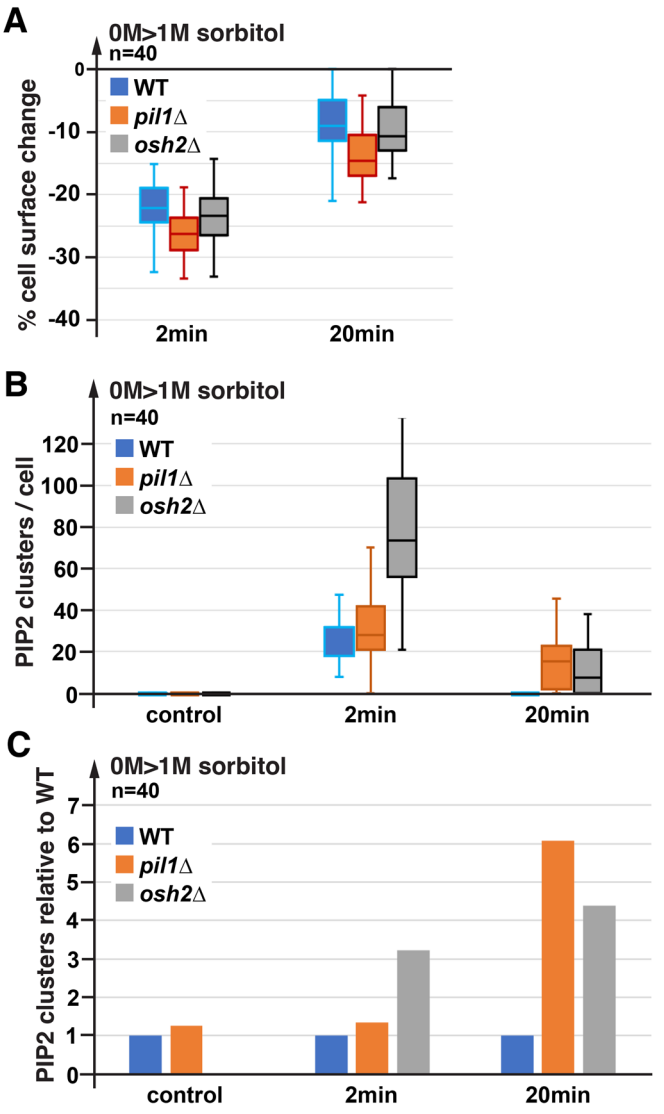

FIGURE 11: Eisosome and lipid-transfer mutants exhibit delayed recovery of PM tension. (A) Cell surface changes as a consequence of hyperosmotic shock were determined based on diameter measurements of cells observed in a microfluidics chamber. The following strains were used: WT (SEY6210 pJK30), *pil1*Δ (AMY42 pJK30), *osh2*Δ (MTY42 pJK30). The WT data are identical to those in Figure 1A. (B) Strains (SEY6210, AMY42, MTY42) expressing GFP-tagged PIP2 sensor (pCS189) were observed in a microfluidics chamber and the number of PIP2 clusters was counted at different time points after hyperosmotic shock (box-and-whisker blot indicating mean). (C) The same data as shown in B are represented relative to WT (WT = 1).

recovery of membrane tension, which plays an important role in restoring normal functionality of the PM. However, it should be noted that under nutrient-rich conditions (as used in our experiments), 20–30 min after hyperosmotic shock glycerol synthesis will restore cell size, which will also recover PM tension. Therefore, the PM morphology and lipid transport mechanisms we observed likely play an important role in restoring PM function faster, particularly under nutrient limited conditions where glycerol synthesis is limited.

DISCUSSION

We used hyperosmotic shock to study the role of membrane tension on the organization of the PM and on its associated functions. Figure 12A summarizes our observations. The addition of 1M sorbitol to the growth medium resulted in a rapid loss of cell size, causing a ~22% surface area reduction in <20 s. With ~4 s delay relative to the cell size changes, the PM lipid PIP2 started to cluster, indicating phase segregation of the PM. This lipid clustering was completed in <10 s. PIP2 is an essential factor for the formation of endocytic structures. Therefore, the sequestration of PIP2 into large membrane domains is a likely reason for the observed block of endocytosis during the initial phase of the hyperosmotic stress. However, within 10 min, PIP2 clusters dissolved and endocytosis restarted, suggesting that PM tension was back in physiological range. Finally, 20 min after the hyperosmotic shock, glycerol synthesis had restored osmotic balance, which allowed the cells to recover most of their size.

Because cell-size recovery was slow and endocytosis was impaired by the phase segregation of the membrane, other mechanisms had to be responsible for the recovery of PM tension. One mechanism we identified relied on morphology changes of eisosomes, membrane furrows that have been shown to be involved in membrane tension regulation (Kabeche *et al.*, 2015; Appadurai *et al.*, 2020; Ng *et al.*, 2020; Lemiere *et al.*, 2021). In less than 1 min, hyperosmotically stressed cells formed LEDS and within 5 min Pil1-marked eisosomes of the stressed cells doubled in length (Figure 12B). These morphology changes of the PM are predicted to absorb ~70% of the excess membrane.

The membrane domain associated with eisosomes is thicker and more organized than the surrounding membrane (Grossmann *et al.*, 2007; Stradalova *et al.*, 2009; Bharat *et al.*, 2018). One function of this raft-like membrane is to store nutrient transporters in an inactive state (Moharir *et al.*, 2018). Our observations suggested that loss of membrane tension caused the rapid expansion of the eisosomal membrane domain, resulting in large clusters that sequestered most of the PIP2, PS and nutrient transporters. This clustering of the negatively charged lipids PIP2 and PS is consistent with previously published studies that observed enrichment of these lipids in eisosomes (Kefauver *et al.*, 2024; Tsuji *et al.*, 2025). We postulate that the rapid expanding eisosomal membrane fuses with the PM, resulting in the unusual morphology of LEDS (see models in Figures 8 and 12B). Shortly after LEDS form, they start to disappear, which is likely the consequence of the re-establishing of PM tension. Because the formation of LEDS includes membrane fusion, dissolving LEDS requires a membrane fission reaction, which could be accomplished by ESCRT-mediated severing of the membrane tube.

The clustering of PIP2 has been previously described, both in hyperosmotically shocked cells and in cells exposed to the PM intercalating compound palmitoylcarnitine, two treatments that cause loss of PM tension (Riggi *et al.*, 2018). Using EM, this study also identified large PM invaginations, referred to as PES, that seemed to correspond to the LEDS we observed. Furthermore, the study showed that PIP2 clustering at the PES resulted in recruitment and inactivation of TORC2, which ultimately inhibited sphingolipid synthesis at the ER. Together, this previous study and our observations are in good agreement, highlighting the fact that the PM itself senses and responds to the changes in tension.

In addition to the morphology changes of the PM, lipid transport from the PM to the cER also aids in the recovery of PM tension after hyperosmotic stress. This statement is inferred from the

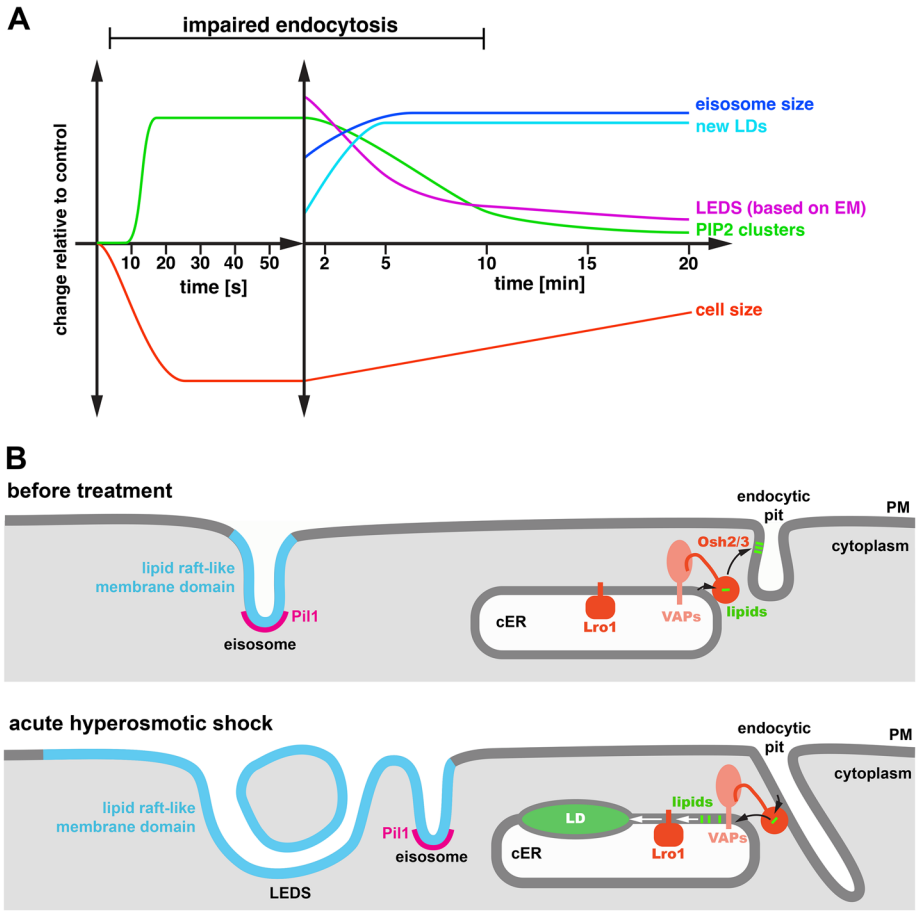

FIGURE 12: Summary and model of the observed responses of yeast during acute hyperosmotic shock. (A) Summary of the observed effects of hyperosmotic shock on PM morphology, lipid clustering, and LD formation (note the two different time axes). (B) Model of the PM morphology changes and the lipid transfer caused by the acute hyperosmotic-induced drop in PM tension.

observations that hyperosmotic shock caused the rapid (<5 min) formation of new LDs at the cER and that this LD formation was dependent on the lipid-transport proteins Osh2 and Osh3. Furthermore, LD formation required the membrane contact site proteins Scs2 and Scs22 that function in the recruitment of Osh2/3 to ER-PM contact sites, and the acyltransferase, Lro1. These observations suggested that lipids from the low-tension PM were transported by Osh2/3 via contact sites to the cER where they were modified by Lro1 and shunted into LDs (see model in Figure 12B). Osh2/3 together with the VAPs Scs2/22 have been implicated in the transport of ergosterol from the cER to sites of endocytosis. This sterol transport was shown to be important for the actin polymerization at the endocytic pit and for the efficient formation of endocytic vesicles (Encinar Del Dedo *et al.*, 2017). In contrast, low PM tension seemed to reverse the direction of Osh2/3-Scs2/22–mediated lipid transport (Figure 12B), thereby removing lipids from endocytic sites, which might help restore endocytosis. The fact that Lro1 was required for hyperosmotic-induced LD formation indicated that mainly glycerophospholipids and not sterols were shunted into the newly formed LDs. Therefore, during hyperosmotic-induced lipid transport, Osh2/3 might have changed their specificity from ergosterol to other lipids. Alternatively, the Osh2/3-mediated transport of ergosterol from the PM to the cER might change the local ER lipid composition in a way that promoted the formation of new triacylglycerol-containing LDs.

In summary, our study showed that eisosomes and EPCSs are part of an immediate response system that tries to restore PM tension by morphology change (forming LEDS) and by the transport of PM lipids from endocytic sites to the cER. This stress response we observed by the addition of 1M sorbitol is likely an extreme version of the homeostatic mechanisms that maintain membrane tension under all conditions. It is likely that eisosomes continuously change their size to adjust for fluctuations in membrane tension. Similarly, lipid transport in and out of endocytic sites might locally adjust membrane tension to allow for efficient endocytosis. Losing these mechanisms resulted in delayed recovery of PM tension from the hyperosmotic shock, which likely represents a strong survival disadvantage in the dynamic environment of a wild yeast.

MATERIALS AND METHODS

Request a protocol through *Bio-protocol*

Yeast cultures, growth conditions, and plasmids

Yeast strains were grown at 30°C in synthetic dextrose medium (SD; yeast nitrogen base, 2% glucose) in presence of all amino acids and necessary supplements, except in case of plasmid selection. The strains and plasmids used in this study are listed in Table 1. Expression of constructs using the *CUP1* promoter were induced by the addition of 0.1 mM $CuSO_4$. Deletion or tagging

Strains	Descriptive name	Genotype or description	Reference or source
SEY6210	WT	*MATα leu2-3,112 ura3-52 his3-Δ200 trp1-Δ901 lys2-801 suc2-Δ9 GAL*	(Robinson *et al.*, 1988)
AMY6	*PIL1-mCherry*	SEY6210, *PIL1-mCherry, KANMX6*	(Moharir *et al.*, 2018)
AMY42	*pil1Δ*	SEY6210, *PIL1::KANMX6*	(Moharir *et al.*, 2018)
MTY42	*osh2Δ*	SEY6210, *OSH2::TRP1*	This study
MTY43	*osh3Δ*	SEY6210, *OSH2::KANMX6*	This study
JPY47	*are1Δ, are2Δ*	SEY6210, *ARE1::KANMX6, ARE2::TRP1*	This study
JPY23	*lro1Δ*	SEY6210, *LRO1::TRP1*	This study
JPY15	*scs2Δ, scs22Δ*	SEY6210, *SCS2::KANMX6, SCS22::TRP1*	This study
JPY22	*dga1Δ*	SEY6210, *DGA1::TRP1*	This study
JPY35	*ERG6-GFP*	SEY6210, *ERG6-GFP, TRP1*	This study
JPY38	*PIL1-mCherry, ERG6-GFP*	AMY6, *ERG6-GFP, TRP1*	This study
JPY45	*tcb1Δ, tcb2Δ, tcb3Δ*	SEY6210, *TCB1:: KANMX6, TCB2::HIS3, TCB3::TRP1*	This study
BWY1346	*end3Δ*	SEY6210, *end3Δ*	(Whitworth *et al.*, 2014)
BWY3817	*MUP1-GFP*	SEY6210, *MUP1-GFP, TRP1*	(Prosser *et al.*, 2010)
Plasmids			
pJK30	*FUR4(ΔN)-GFP*	*URA3* (pRS416) P(*CUP1*)-*fur4(ΔN)-GFP*	(Keener and Babst, 2013)
pCS189	GFP-2xPH	*URA3* (pRS426) P(*PRC1*)-*GFP-2xPH*	(Stefan *et al.*, 2002)
pPL4146	*MUP1-GFP*	*LEU2* (pRS315) P(*CUP1*)-*MUP1-GFP*	(Stringer and Piper, 2011)
pGFP-C2(Y)	*GFP-C2*	*URA3* (pRS426) *P(PRC1)-GFP-Lactadherin C2 (Bovine)*	Mark Lemmon
pCG1	*mCherry-2xPH*	*URA3* (pRS426) *mCherry-2xPH*	(Riggi *et al.*, 2018)

TABLE 1: Strains and plasmid.

of chromosomal genes was performed by homologues recombination (Longtine *et al.*, 1998). Genomic modifications were confirmed by PCR.

Fluorescence microscopy

Cells were inoculated from a plate the day prior and grown overnight into late log phase/early stationary phase in proper defined media. In the morning, cells were then diluted to an optical density at 600 nm (OD_{600}) of 0.1 into 5 ml of media. Cultures were then allowed to grow to midlog phase, $OD_{600} = 0.8$. For direct imaging, 500 µl of the culture were concentrated by centrifugation at for 1 min at 3000 × *g*. Media was aspirated down to 20–40 µl of cell pellet. Of the concentrated cell suspension, 2 µl were then added to a glass slide and spread with a coverslip. Imaging using the microfluidics system (CellASIC ONIX, Millipore Sigma) was performed at 30°C with constant flow of medium at 4 psi. An Olympus deconvolution microscope with a 100x objective in immersion oil was used to generate Z-stacks (0.3 µm). For staining with FM4-64, the growth medium contained 40 mM MES pH5.5. The FM4-64 dye was added at 10 µM to the medium in the microfluidics plate. The microscopy pictures of the controls (before hyperosmotic shock) were taken after ∼30 s of staining, before the cells were switched into medium containing 1M sorbitol and 10 µM FM4-64. It should be noted that the surface of the microfluidics chamber is hydrophobic and thus absorbs the FM4-64 dye. Therefore, the microfluidics chamber has to be preflushed for 20 min with the dye-containing medium before the experiment can be performed. Furthermore, the concentration of the free dye in the medium of the chamber is likely reduced.

To quantify Erg6-GFP structures, Z stacks were deconvoluted and projected into whole cells. These images were then loaded into Olympus Cellsens Dimension software. Cells were first labeled as objects. These objects were then converted to regions of interest (ROI's) and copied from the images of positions before treatment, to the appropriate plate position of timepoints after treatment start. Erg6-GFP puncta were then masked using the Adaptive threshold function. Then, Erg6-GFP puncta that were spatially too close and counted as one object, were manually split. Finally, the number of objects per ROI were counted using the "Count and Measure" operation contained within Olympus Cellsens Dimension software. Quantification of PIP2 dots of deconvoluted and collapsed Z stacks was done manually. Cell size measurements were performed manually using the Olympus Cellsens Dimension software.

Quantification of Mup1 internalization was performed on deconvolved cross-sections (300 nm optical section trough the center of the cell). The Magic Wand tool in the Photoshop software package was used to outline the cells and to quantify the total fluorescence intensity of the cell. The intracellular signal, excluding the PM, was obtained by retracting in Photoshop the cell outline by 6 pixels (PM signal = total minus intracellular).

BODIPY staining of LDs and quantification

Cells were grown to midlogarithmic phase for 24–48 h in defined medium containing 2% galactose as carbon source. Cells grown in galactose have less LDs and thus are easier to analyze and quantify. For treatment, 150 µl of culture, 50 µl of 4M sorbitol, and 2 µl of 200 µM BODIPY (4,4-difluoro-4-bora-3a,4a-diaza-s-indacene) were combined into an Eppendorf tube and incubated at 30°C for 20 min. For the control sample, 200 µl of cells and 2 µl 200 µM BODIPY were incubated under the same conditions. Cells were then concentrated and whole cell Z-stacks were imaged with fluorescent microscopy on a slide. Images were deconvoluted, projected, and imported into Fiji, TrakEM2. A circular mask was set as the object diameter and the object was then placed over each LD of 50–60 cells for each treatment group. For larger BODIPY-stained areas of incongruous shape, the presized LD marker, was used to fill in said fluorescent area to account for LD number loss due to the limits of light diffraction.

EM

Overnight cultures were diluted in 10 ml of synthetic complete medium to $OD_{600} = 0.1$ and grown to midlogarithmic phase ($OD_{600} = 0.8$). The hyperosmotically shocked samples were treated by the addition 4M sorbitol to a final concentration of 1M sorbitol for various timepoints. Upon reaching the timepoint, cells were chemically fixed and 50 nm cryo-sections were obtained as described before (Appadurai *et al.*, 2020). For estimating the number of eisosome, LEDS and large eisosome-like invaginations per cell, the average number of these structures observed in 40 cell cross-sections was divided by the surface area of the cross-sections (circumference x 50 nm). These numbers (structure/μm^2) were multiplied by the average surface area of the cells hyperosmotically shocked cells observed by fluorescence microscopy (data used for Figure 1A; t = 0 68 μm^2, t = 1 min 54 μm^2, t = 5 min 54 μm^2, t = 10 min 55 μm^2). Because eisosomes and their derived structures are estimated to be ~300 nm in length (Stradalova *et al.*, 2009), we divided the numbers by 6 (6x50 nm sections) to obtain our estimated number of structures per cell.

REFERENCES

Appadurai D, Gay L, Moharir A, Lang MJ, Duncan MC, Schmidt O, Teis D, Vu TN, Silva M, Jorgensen EM, *et al.* (2020). Plasma membrane tension regulates eisosome structure and function. Mol Biol Cell 31, 287–303.

Benedetti H, Raths S, Crausaz F, Riezman H (1994). The END3 gene encodes a protein that is required for the internalization step of endocytosis and for actin cytoskeleton organization in yeast. Mol Biol Cell 5, 1023–1037.

Bharat TAM, Hoffmann PC, Kukulski W (2018). Correlative microscopy of vitreous sections provides insights into BAR-domain organization in situ. Structure 26, 879–886.e3.

Blomberg A (2022). Yeast osmoregulation - glycerol still in pole position. FEMS Yeast Res 22, foac035.

De Belly H, Stubb A, Yanagida A, Labouesse C, Jones PH, Paluch EK, Chalut KJ (2021). Membrane tension gates ERK-mediated regulation of pluripotent cell fate. Cell Stem Cell 28, 273–284.e6.

Douglas LM, Konopka JB (2014). Fungal membrane organization: The eisosome concept. Annu Rev Microbiol 68, 377–393.

Encinar Del Dedo J, Idrissi FZ, Fernandez-Golbano IM, Garcia P, Rebollo E, Krzyzanowski MK, Grotsch H, Geli MI. (2017). ORP-mediated ER contact with endocytic sites facilitates actin polymerization. Dev Cell 43, 588–602.e6.

Grossmann G, Opekarova M, Malinsky J, Weig-Meckl I, Tanner W (2007). Membrane potential governs lateral segregation of plasma membrane proteins and lipids in yeast. EMBO J 26, 1–8.

Kabeche R, Howard L, Moseley JB (2015). Eisosomes provide membrane reservoirs for rapid expansion of the yeast plasma membrane. J Cell Sci 128, 4057–4062.

Keener JM, Babst M (2013). Quality control and substrate-dependent downregulation of the nutrient transporter fur4. Traffic 14, 412–427.

Kefauver JM, Hakala M, Zou L, Alba J, Espadas J, Tettamanti MG, Gajic J, Gabus C, Campomanes P, Estrozi LF, *et al.* (2024). Cryo-EM architecture of a near-native stretch-sensitive membrane microdomain. Nature 632, 664–671.

Kozlov MM, Chernomordik LV (2015). Membrane tension and membrane fusion. Curr Opin Struct Biol 33, 61–67.

Le Roux AL, Quiroga X, Walani N, Arroyo M, Roca-Cusachs P (2019). The plasma membrane as a mechanochemical transducer. Philos Trans R Soc Lond B Biol Sci 374, 20180221.

Leber R, Zinser E, Zellnig G, Paltauf F, Daum G (1994). Characterization of lipid particles of the yeast, Saccharomyces cerevisiae. Yeast 10, 1421–1428.

Lemiere J, Ren Y, Berro J (2021). Rapid adaptation of endocytosis, exocytosis, and eisosomes after an acute increase in membrane tension in yeast cells. Elife 10, e62084.

Longtine MS, McKenzie A 3rd, Demarini DJ, Shah NG, Wach A, Brachat A, Philippsen P, Pringle JR (1998). Additional modules for versatile and economical PCR-based gene deletion and modification in Saccharomyces cerevisiae. Yeast 14, 953–961.

Moharir A, Gay L, Appadurai D, Keener J, Babst M (2018). Eisosomes are metabolically regulated storage compartments for APC-type nutrient transporters. Mol Biol Cell 29, 2113–2127.

Ng AQE, Ng AYE, Zhang D (2020). Plasma membrane furrows control plasticity of ER-PM contacts. Cell Rep 30, 1434–1446.e7.

Oelkers P, Tinkelenberg A, Erdeniz N, Cromley D, Billheimer JT, Sturley SL (2000). A lecithin cholesterol acyltransferase-like gene mediates diacylglycerol esterification in yeast. J Biol Chem 275, 15609–15612.

Pettersson N, Filipsson C, Becit E, Brive L, Hohmann S (2005). Aquaporins in yeasts and filamentous fungi. Biol Cell 97, 487–500.

Prosser DC, Whitworth K, Wendland B (2010). Quantitative analysis of endocytosis with cytoplasmic pHluorin chimeras. Traffic 11, 1141–1150.

Qian T, Li C, He R, Wan C, Liu Y, Yu H (2021). Calcium-dependent and -independent lipid transfer mediated by tricalbins in yeast. J Biol Chem 296, 100729.

Riggi M, Niewola-Staszkowska K, Chiaruttini N, Colom A, Kusmider B, Mercier V, Soleimanpour S, Stahl M, Matile S, Roux A, *et al.* (2018). Decrease in plasma membrane tension triggers PtdIns(4,5)P2 phase separation to inactivate TORC2. Nat Cell Biol 20, 1043–1051.

Robinson JS, Klionsky DJ, Banta LM, Emr SD (1988). Protein sorting in *Saccharomyces cerevisiae*: Isolation of mutants defective in the delivery and processing of multiple vacuolar hydrolases. Mol Cell Biol 8, 4936–4948.

Roffay C, Molinard G, Kim K, Urbanska M, Andrade V, Barbarasa V, Nowak P, Mercier V, Garcia-Calvo J, Matile S, *et al.* (2021). Passive coupling of membrane tension and cell volume during active response of cells to osmosis. Proc Natl Acad Sci U S A 118, e2103228118.

Rollenhagen C, Agyeman H, Eszterhas S, Lee SA (2022). Candida albicans END3 mediates endocytosis and has subsequent roles in cell wall integrity, morphological switching, and tissue invasion. Microbiol Spectr 10, e0188021.

Saito H, Posas F (2012). Response to hyperosmotic stress. Genetics 192, 289–318.

Sitarska E, Diz-Munoz A (2020). Pay attention to membrane tension: Mechanobiology of the cell surface. Curr Opin Cell Biol 66, 11–18.

Stefan CJ, Audhya A, Emr SD (2002). The yeast synaptojanin-like proteins control the cellular distribution of phosphatidylinositol (4,5)-bisphosphate. Mol Biol Cell 13, 542–557.

Stradalova V, Stahlschmidt W, Grossmann G, Blazikova M, Rachel R, Tanner W, Malinsky J (2009). Furrow-like invaginations of the yeast plasma membrane correspond to membrane compartment of Can1. J Cell Sci 122, 2887–2894.

Stringer DK, Piper RC (2011). A single ubiquitin is sufficient for cargo protein entry into MVBs in the absence of ESCRT ubiquitination. J Cell Biol 192, 229–242.

Tsuji T, Hasegawa J, Sasaki T, Fujimoto T (2025). Definition of phosphatidylinositol 4,5-bisphosphate distribution by freeze-fracture replica labeling. J Cell Biol 224, e202311067.

Walther TC, Brickner JH, Aguilar PS, Bernales S, Pantoja C, Walter P (2006). Eisosomes mark static sites of endocytosis. Nature 439, 998–1003.

Wendland B, McCaffery JM, Xiao Q, Emr SD (1996). A novel fluorescence activated cell sorter based screen for yeast. J Cell Biol 135, 1485–1500.

Whitworth K, Bradford MK, Camara N, Wendland B (2014). Targeted disruption of an EH-domain protein endocytic complex, Pan1-End3. Traffic 15, 43–59.